Unsteady MHD Mixed Convection Flow in Hybrid Nanofluid at Three-Dimensional Stagnation Point

Nurul Amira Zainal [1,2], **Roslinda Nazar** [1], **Kohilavani Naganthran** [1,*] **and Ioan Pop** [3]

[1] Department of Mathematical Sciences, Faculty of Science Technology, Universiti Kebangsaan Malaysia, 43600 UKM, Bangi 43600, Selangor, Malaysia; nurulamira@utem.edu.my (N.A.Z.); rmn@ukm.edu.my (R.N.)

[2] Fakulti Teknologi Kejuruteraan Mekanikal dan Pembuatan, Universiti Teknikal Malaysia Melaka, Hang Tuah Jaya, Durian Tunggal 76100, Melaka, Malaysia

[3] Department of Mathematics, Babeş-Bolyai University, R-400084 Cluj-Napoca, Romania; popm.ioan@yahoo.co.uk

[*] Correspondence: kohi@ukm.edu.my

Abstract: There has been significant interest in exploring a stagnation point flow due to its numerous potential uses in engineering applications such as cooling of nuclear reactors. Hence, this study proposed a numerical analysis on the unsteady magnetohydrodynamic (MHD) mixed convection at three-dimensional stagnation point flow in Al_2O_3–Cu/H_2O hybrid nanofluid over a permeable sheet. The ordinary differential equations are accomplished by simplifying the governing partial differential equations through suitable similarity transformation. The numerical computation is established by the MATLAB system software using the bvp4c technique. The bvp4c procedure is excellent in providing more than one solution once sufficient predictions are visible. The influence of certain functioning parameters is inspected, and notable results exposed that the rate of heat transfer is exaggerated along with the skin friction coefficient while the suction/injection and magnetic parameters are intensified. The results also signified that the rise in the volume fraction of the nanoparticle and the decline of the unsteadiness parameter demonstrates a downward attribution towards the heat transfer performance and skin friction coefficient. Conclusively, the observations are confirmed to have multiple solutions, which eventually contribute to an investigation of the analysis of the solution stability, thereby justifying the viability of the first solution.

Keywords: magnetohydrodynamic; stagnation point; stability analysis; hybrid nanofluid; mixed convection

1. Introduction

The observation of magnetohydrodynamic (MHD) flow behavior is essential in diverse fields of engineering and has attracted considerable attention due to its significance in industrial applications, for instance in fossil-fueled power generation [1]. The existence of MHD in a fluid that conducts electricity gives rise to a resistive type force, which causes the fluid particle's motion resistance knows as Lorentz force. The Lorentz force intensifies the fluid temperature and concentration significantly, thereby slowing down the boundary layer's separation. The analysis throughout unsteady MHD flow at the forward stagnation point was first triggered by Katagiri [2]. Pavlov [3] developed the study of an electrically conducting MHD fluid in the boundary layer, including a transverse magnetic field related to a stretching sheet. The research was expanded by Takhar and Gupta [4] who testified the stabilizing effect detection on Taylor-Görtler three-dimensional disturbances and reviewed the solution stability in the magnetic field. Ever since a substantial number of studies with the consideration of MHD have been performed including [5–8]. Such research, however, has exempted the mixed convection flow.

Convective heat transfer, also known as convection, is a phenomenon where the flow of fluids transfers heat from one position to the next. The process under which an

external source induces fluid motion is called forced convection. Free or normal convection, alternatively, is a process in which buoyancy forces alone produce fluid motion, arising from density differences. When both natural and forced convection systems function together, mixed convection mechanism occurs. The topic of mixed convection flow has drawn much interest from the researchers because of its prominence in manufacturing industries, for example, solar and nuclear collectors, heat exchangers, and atmospheric boundary layer flows [9]. The groundbreaking work on numerical analysis of mixed convection stagnation point flow past heated vertical flat surfaces was performed by Ramachandran et al. [10]. They extended the work done by Merkin [11] who found a non-uniqueness solution within a specific range of mixed convection parameter. The research was then broadened by Merkin [12] in his next exploration, where the stability of the results has been identified. Since then, a significant number of publications on mixed convection with the presence of MHD have been produced. Oztop et al. [13] performed MHD mixed convection laminar flow in a lid-driven cavity, Daniel and Daniel [14] investigated the MHD mixed convection flow with thermal radiation effect towards a stretching porous surface by utilizing the homotopy analysis method while Jamaludin et al. [15] examined the influence of the heat source/sink in MHD mixed convection stagnation point in a hybrid nanofluid. It is found that the heat transfer of the conventional alumina/water nanofluid is greater than then copper–alumina water nanofluid with the increment in the heat source/sink parameter.

To provide better-evolved heat conductivity, an innovative type of nanofluid introduced as hybrid nanofluid is invented. This alternative form of working fluid has now captivated many scientists due to its popularity in thermal properties advancement [16–18]. Specifying a good nanoparticles mixture is part of the main components in maintaining a robust nanofluid hybrid suspension. Xian et al. [19] and Gupta et al. [20] has studied the hybrid nanoparticle preparation method and the stabilization mechanism as well as its importance in the industrial sectors. Suresh et al. [21] conducted an exploratory practice to analyze the thermophysical characteristics of Al_2O_3–Cu/H_2O hybrid nanofluid. Their discovery reveals that the stability of hybrid nanofluid depends mostly on the concentration of nanoparticles and the stability of higher-concentration nanofluid is incompetent. Consequently, the experimental results disclose Al_2O_3–Cu/H_2O is capable of increasing thermal conductivity efficiency and reliability. In another report, Suresh et al. [22] used different concentrations of nanocomposite powder in Al_2O_3–Cu/H_2O to conduct the synthesis, characterization and stability. The stability of prepared nanofluid is observed to decrease when the volume concentration is increased. Since hybrid nanofluid is claimed to have a range of beneficial characteristics in improving thermal conductivity, many researchers performed an investigation on the hybrid nanofluid by considering diverse aspect and conditions [23–27].

Researchers have widely studied the stagnation point flow focused on its uses in engineering areas and sectors such as wire drawing, paper making, hot rolling, and several others. The stagnation point flow field and heat transfer can be used to verify the consistency of certain goods. The flow of stagnation points was initially proposed by Hiemenz [28] in 1911. To tackle the two-dimensional stagnation point flow, he employed the similarity variables and achieved the exact solution to the problems. Afterwards, Libby [29] performed a boundary layer analysis on heat and mass transfer in three-dimensional stagnation point flow. Chiam [30] revealed the stagnation point flow analysis against a stretching sheet and expanded his study on heat transport analysis using the regular perturbation technique in stagnation point flow. Earlier stages of mixed convection flow in stagnation point flow have been studied by Takhar [31] in an incompressible fluid. Chamkha [32] studied continuous, two-dimensional, MHD mixed convection flows near a stagnation point of an electrically conducting and heat-absorbing fluid on a semi-infinite vertical permeable surface with arbitrary variations of surface heat flux. Meanwhile, Abdelkhalek [33] performed a numerical analysis to examine the impact of mass transfer in MHD mixed convection in view of stagnation point flow over a heated vertical permeable sheet. Jamaludin et al. [34] scrutinized the stability analysis of the mixed

convection phenomenon toward a nonlinearly permeable surface. Researchers reviewed some recent inspections based on stagnation point flow through [35–39].

The overarching focus of this study is to conduct an analysis on unsteady MHD mixed convection stagnation point in the three-dimensional flow of alumina-copper/water hybrid nanofluid with stability analysis. According to the works described above, this propose problem remains briefly addressed in the literature. The idea of the present article was motivated by Noor et al. [40] and the evaluation was carried out by applying the bvp4c feature to obtain non-uniqueness solutions in the opposing flow past a permeable surface. The combination of alumina and copper nanoparticle were chosen in this study based on the outstanding works of Suresh et al. [21,22] as discussed earlier. The correlations properties of hybrid nanofluid are employed inspired by Takabi and Salehi [41] and Ghalambaz et al. [42]. The present work applied the bvp4c tool in the MATLAB platforms to address the constructed problem. More than one solution has been productively recognized by the stated approach method. In addition, analysis of solution stability is conducted to verify the solutions constancy for a valid physical explanation. This major participation will lead to stimulating industrial progress, particularly in the engineering and manufacturing sectors.

2. Mathematical Modeling

The current work considers unsteady MHD mixed convection near the stagnation point in the three-dimensional flow of Al_2O_3–Cu/H_2O hybrid nanofluid. In this problem, u, v and w are the velocity component through $x-, y-$ and $z-$ axes with the origin at the nodal stagnation point N, as displayed in Figure 1. $T_{wx}(x, t)$ and $T_{wy}(y,t)$ are the variable temperatures, and T_∞ is the surrounding fluid temperature, where $T_{wx}(x, t)$, $T_{wy}(y, t) < T_\infty$ denote the opposing flow and $T_{wx}(x, t)$, $T_{wy}(y, t) > T_\infty$ apply to the assisting flow. We assume that $T_{wx}(x) = T_\infty + \left(T_0(x/L)/(1 - \delta t)^2\right)$ and $T_{wx}(y) = T_\infty + \left(T_0(y/L)/(1 - \delta t)^2\right)$, where T_0 is the characteristic temperature of the surface of the sheet, with $T_0 > 0$ for assisting flow and $T_0 < 0$ denotes the opposing flow, while L is the characteristic length of the surface of the sheet. Here, δ is a parameter showing the unsteadiness of the problem towards t, time. Generally, $\delta = 0$ signifies the steady inviscid flow, $\delta > 0$ accelerates the outer potential flow, while $\delta < 0$ corresponds to the reverse flow. The outer flow is assumed to be $u_e(x) = ax/(1 - \delta t)$ and $v_e(x) = by/(1 - \delta t)$ in $x-$ and $y-$ axes, respectively. Noticeably, $c = b/a$, where c represents the three-dimensional stagnation points parameter or ratio of velocity gradients at the edge of the boundary layer, with a and b are the principal curvatures parameter at N or the velocity gradients at the edge of the boundary layer along the $x-$ and $y-$ axes, respectively [43,44]. Both a, b are positive constants. Further, $b = a$ corresponds to the axisymmetric case, while $b = 0$ is the plane stagnation flow problem. If a, b are positive, the solution of the corresponding equations results in nodal points of attachment, that is, $0 \leq c \leq 1$. On the contrary, the saddle points of attachment are declared if a and b are negative, that is, $-1 \leq c \leq 0$. Also, it should be noted that when $c = 0$, the problem will convert to a two-dimensional case, while the axisymmetric case can be regained as $c = 1$. The plane of the body remains stagnant and there is a mass flux velocity denoted by w_0 as the surface is permeable, with $w_0 > 0$ referring to injection and $w_0 < 0$ representing the suction condition. The transverse magnetic field $B^2(x) = B_0^2/(1 - \delta t)$ is considered normal, where B_0 is the magnetic field strength. From the above assumptions, the governing boundary layer equations can be defined as [9,43]:

$$\frac{\partial u}{\partial x} + \frac{\partial v}{\partial y} + \frac{\partial w}{\partial z} = 0 \tag{1}$$

$$\frac{\partial u}{\partial t} + u\frac{\partial u}{\partial x} + v\frac{\partial u}{\partial y} + w\frac{\partial u}{\partial z} = \frac{\partial u_e}{\partial t} + u_e\frac{du_e}{d_x} + \frac{\mu_{hnf}}{\rho_{hnf}}\frac{\partial^2 u}{\partial z^2} + \frac{(\rho\beta)_{hnf}}{\rho_{hnf}}(T - T_\infty)g - \frac{\sigma_{hnf}B^2}{\rho_{hnf}}(u - u_e) \tag{2}$$

$$\frac{\partial v}{\partial t} + v\frac{\partial v}{\partial x} + v\frac{\partial v}{\partial y} + w\frac{\partial v}{\partial z} = \frac{\partial v_e}{\partial t} + v_e\frac{dv_e}{d_x} + \frac{\mu_{hnf}}{\rho_{hnf}}\frac{\partial^2 v}{\partial z^2} + \frac{(\rho\beta)_{hnf}}{\rho_{hnf}}(T - T_\infty)g - \frac{\sigma_{hnf}B^2}{\rho_{hnf}}(v - v_e) \tag{3}$$

$$\frac{\partial T}{\partial t} + u\frac{\partial T}{\partial x} + v\frac{\partial T}{\partial y} + w\frac{\partial T}{\partial z} = \frac{k_{hnf}}{(\rho C_p)_{hnf}}\frac{\partial^2 T}{\partial z^2}, \tag{4}$$

together with:

$$\begin{aligned} t < 0 &: u = 0, \quad v = 0, \quad w = 0, \quad T = T_\infty \text{ for any } x, y, z = 0, \\ t \geq 0 &: u = 0, \quad v = 0, \quad w = w_0, \quad T = T_w \text{ at } z = 0, \\ & u \rightarrow u_e(x), v \rightarrow v_e(x), \quad T \rightarrow T_\infty \text{ as } z \rightarrow \infty. \end{aligned} \tag{5}$$
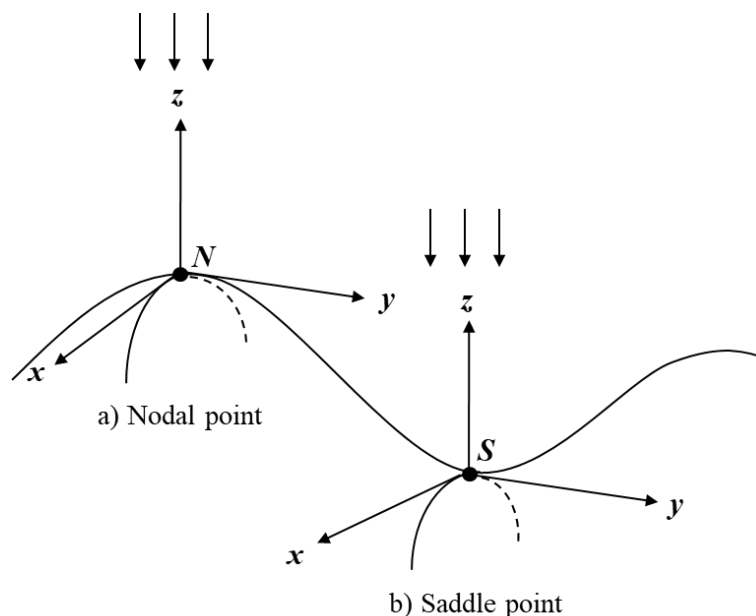
Figure 1. The schematic model.

At this point, g is the acceleration to gravity, μ_{hnf} is the Al$_2$O$_3$–Cu/H$_2$O dynamic viscosity, k_{hnf} and ρ_{hnf} are the Al$_2$O$_3$–Cu/H$_2$O thermal/heat conductivity and density, respectively, σ_{hnf} is the electrical conductivity, and finally $(\rho C_p)_{hnf}$ is the heat capacity of Al$_2$O$_3$–Cu/H$_2$O. Table 1 provides the correlation properties of Al$_2$O$_3$–Cu/H$_2$O as established by [41,42] while Table 2 presents the thermophysical properties [45] of the working fluid.

Then, we introduce the subsequent similarity transformations which are provided as [40,46]:

$$u = \frac{af'}{1 - \delta t}x, \ v = \frac{bh'}{1 - \delta t}y, \ w = -\sqrt{\frac{av}{1 - \delta t}}[f(\eta) + ch(\eta)],$$

$$\theta = \frac{T - T_\infty}{T_w - T_\infty}, \ \eta = \sqrt{\frac{a}{v(1 - \delta t)}}z, \tag{6}$$

Table 1. The Al$_2$O$_3$–Cu/H$_2$O correlation properties.

Properties	Al$_2$O$_3$–Cu/H$_2$O
Density	$\rho_{hnf} = \left(1 - \phi_{hnf}\right)\rho_f + \phi_1\rho_{s1} + \phi_2\rho_{s2}$
Thermal capacity	$(\rho C_p)_{hnf} = \left(1 - \phi_{hnf}\right)(\rho C_p)_f + \phi_1(\rho C_p)_{s1} + \phi_2(\rho C_p)_{s2}$
Dynamic viscosity	$\mu_{hnf} = 1/\left(1 - \phi_{hnf}\right)^{2.5}$
Electrical conductivity	$\dfrac{\sigma_{hnf}}{\sigma_f} = \left[\dfrac{\left(\dfrac{\phi_1\sigma_{s1} + \phi_2\sigma_{s2}}{\phi_{hnf}}\right) + 2\sigma_f + 2(\phi_1\sigma_{s1} + \phi_2\sigma_{s2}) - 2\phi_{hnf}\sigma_f}{\left(\dfrac{\phi_1\sigma_{s1} + \phi_2\sigma_{s2}}{\phi_{hnf}}\right) + 2\sigma_f - (\phi_1\sigma_{s1} + \phi_2\sigma_{s2}) + \phi_{hnf}\sigma_f}\right]$
Thermal conductivity	$\dfrac{k_{hnf}}{k_f} = \left[\dfrac{\left(\dfrac{\phi_1 k_{s1} + \phi_2 k_{s2}}{\phi_{hnf}}\right) + 2k_f + 2(\phi_1 k_{s1} + \phi_2 k_{s2}) - 2\phi_{hnf}k_f}{\left(\dfrac{\phi_1 k_{s1} + \phi_2 k_{s2}}{\phi_{hnf}}\right) + 2k_f - (\phi_1 k_{s1} + \phi_2 k_{s2}) + \phi_{hnf}k_f}\right]$

Table 2. The thermophysical properties of working fluid.

Physical Properties	Cu	Al$_2$O$_3$	H$_2$O
k (W/mK)	400	40	0.613
ρ (kg/m^3)	8933	3970	997.1
C_p (J/kgK)	385	765	4179
$\beta \times 10^{-5}$ (mK)	1.67	0.85	21

Substituting Equation (6) into Equations (2)–(5), a series of similarity differential equations may be interpreted as:

$$\frac{\mu_{hnf}/\mu_f}{\rho_{hnf}/\rho_f}f''' + \left(f + ch - \frac{1}{2}\varepsilon\eta\right)f'' - (f' + \varepsilon)f' + \varepsilon + 1 + \frac{\beta_{hnf}}{\beta_f}\Omega\theta - \frac{\sigma_{hnf}/\sigma_f}{\rho_{hnf}/\rho_f}M(f' - 1) = 0, \qquad (7)$$

$$\frac{\mu_{hnf}/\mu_f}{\rho_{hnf}/\rho_f}h''' + \left(f + ch - \varepsilon\frac{1}{2}\eta\right)h'' - (ch' + \varepsilon)h' + \varepsilon + c + \frac{\beta_{hnf}}{\beta_f}\Omega\theta - \frac{\sigma_{hnf}/\sigma_f}{\rho_{hnf}/\rho_f}M(h' - 1) = 0, \qquad (8)$$

$$\frac{1}{\text{Pr}}\frac{k_{hnf}/k_f}{(\rho C_p)_{hnf}/(\rho C_p)_f}\theta'' + \left(f + ch - \varepsilon\frac{1}{2}\eta\right)\theta' - (f' + ch' + 2\varepsilon)\theta = 0, \qquad (9)$$

considering that:

$$f(0) = S, f'(0) = 0, h(0) = 0, h'(0) = 0, \theta(0) = 1,$$
$$f'(\eta) \to 1, h'(\eta) \to 1, \theta(\eta) \to 0, \text{ while } \eta \to \infty. \qquad (10)$$

Here $\varepsilon = \delta/a$ refers to the unsteadiness parameter with $\varepsilon = 0$ signifies steady-state flow, $\varepsilon < 0$ implies the decelerating flow and $\varepsilon > 0$ denotes an accelerating flow and Pr stands for Prandtl number. The solution is obtained numerically and not using perturbation. The effect of ε is very well and in detail presented in Section 4: Discussion and Results. The mixed convection parameter symbolizes by Ω, where $\Omega > 0$ signifies the assisting flow and $\Omega < 0$ suggests an opposing flow, S represents the steady mass flux parameter ($S > 0$ for suction and $S < 0$ for injection) and M is the magnetic coefficient, which are described as

$$\Omega = \frac{Gr}{\text{Re}_x{}^2}, \text{ Pr} = \frac{\nu_f}{\alpha_f}, S = -w_0/\sqrt{a\nu}, M = \frac{B_0{}^2\sigma_f}{a\rho_f}, \qquad (11)$$

where $Gr = g\beta_f(T_w - T_\infty)x^3/\nu_f{}^2$ is the local Grashof number and $Re_x = ax^2/\nu_f(1 - \delta t)$, $Re_y = ay^2/\nu_f(1 - \delta t)$ is the local Reynolds number. Subsequently, the physical quantities of interest are:

$$C_{fx} = \frac{\tau_{wx}}{\rho_f u_e{}^2}, \; C_{fy} = \frac{\tau_{wy}}{\rho_f v_e{}^2}, \; Nu_x = \frac{xq_w}{k_f(T_w - T_\infty)}. \tag{12}$$

Note that C_{fx}, C_{fy} is the skin friction coefficient along $x-$ and $y-$ axes, respectively, and Nu_x is the local Nusselt number. The surface heat flux is identified as q_w, whereas τ_{wx}, τ_{wy} are the shear stresses illustrated by:

$$\tau_{wx} = \mu_{hnf}\left(\frac{\partial u}{\partial z}\right)_{z=0}, \; \tau_{wx} = \mu_{hnf}\left(\frac{\partial v}{\partial z}\right)_{z=0}, q_w = -k_{hnf}\left(\frac{\partial T}{\partial z}\right)_{z=0}. \tag{13}$$

By exerting Equations (6) and (13) into Equation (12), we earn:

$$\sqrt{Re_x}C_{fx} = \frac{\mu_{hnf}}{\mu_f}f''(0), c\sqrt{Re_y}C_{fy} = \frac{\mu_{hnf}}{\mu_f}h''(0), \frac{1}{\sqrt{Re_x}}Nu_x = -\frac{k_{hnf}}{k_f}\theta'(0), \tag{14}$$

provided that $Re_x = ax^2/(1 - \delta t)\nu_f$ and $Re_y = ay^2/(1 - \delta t)\nu_f$.

3. Stability Analysis

A stability analysis is essential to verify the reliability of the obtained solutions since there exist more than one solution in the problem Equations (7)–(10). Following the contributions of [11,47], we introduce a dimensionless time variable τ, associated with the initial value problem. Now, a new conversion of similarity is proposed in accordance with the unsteady-state query as follows:

$$u = \frac{ax}{1 - \delta t}\frac{\partial f}{\partial \eta}(\eta, \tau), \; v = \frac{by}{1 - \delta t}\frac{\partial h}{\partial \eta}(\eta, \tau), \; w = -\sqrt{\frac{a\nu}{1 - \delta t}}[f(\eta, \tau) + ch(\eta, \tau)],$$

$$\theta = \frac{T - T_\infty}{T_w - T_\infty}, \; \eta = \sqrt{\frac{a}{\nu(1 - \delta t)}}z, \; \tau = \frac{at}{1 - \delta t}. \tag{15}$$

Employing Equation (15) into Equations (7)–(9), the subsequent equations are guaranteed:

$$\frac{\mu_{hnf}/\mu_f}{\rho_{hnf}/\rho_f}\frac{\partial^3 f}{\partial \eta^3} + \left(f + ch - \frac{1}{2}\varepsilon\eta\right)\frac{\partial^2 f}{\partial \eta^2} - \left(\varepsilon + \frac{\partial f}{\partial \eta}\right)\frac{\partial f}{\partial \eta} + \varepsilon + 1 + \frac{\beta_{hnf}}{\beta_f}\Omega\theta$$
$$-\frac{\sigma_{hnf}/\sigma_f}{\rho_{hnf}/\rho_f}M\left(\frac{\partial f}{\partial \eta} - 1\right) - (1 + \varepsilon\tau)\frac{\partial^2 f}{\partial \eta\partial \tau} = 0, \tag{16}$$

$$\frac{\mu_{hnf}/\mu_f}{\rho_{hnf}/\rho_f}\frac{\partial^3 h}{\partial \eta^3} + \left(f + ch - \frac{1}{2}\varepsilon\eta\right)\frac{\partial^2 h}{\partial \eta^2} - c\left(\frac{\partial h}{\partial \eta}\right)^2 + \varepsilon\left(1 - \frac{\partial h}{\partial \eta}\right) + c + \frac{\beta_{hnf}}{\beta_f}\Omega\theta$$
$$-\frac{\sigma_{hnf}/\sigma_f}{\rho_{hnf}/\rho_f}M\left(\frac{\partial h}{\partial \eta} - 1\right) - (1 + \varepsilon\tau)\frac{\partial^2 h}{\partial \eta\partial \tau} = 0, \tag{17}$$

$$\frac{1}{Pr}\frac{k_{hnf}/k_f}{(\rho C_p)_{hnf}/(\rho C_p)_f}\frac{\partial^2 \theta}{\partial \eta^2} + \left(f + ch - \varepsilon\frac{1}{2}\eta\right)\frac{\partial \theta}{\partial \eta} - \left(\frac{\partial f}{\partial \eta} + c\frac{\partial h}{\partial \eta} + 2\varepsilon\right)\theta - (1 + \varepsilon\tau)\frac{\partial \theta}{\partial \tau} = 0 \tag{18}$$

subject to:

$$f(0, \tau) = S, \; \frac{\partial f}{\partial \eta}(0, \tau) = 0, h(0, \tau) = 0, \; \frac{\partial h}{\partial \eta}(0, \tau) = 0, \theta(0, \tau) = 1,$$

$$\frac{\partial f}{\partial \eta}(\eta, \tau) \to 1, \; \frac{\partial h}{\partial \eta}(\eta, \tau) \to 1, \; \theta(\eta, \tau) \to 0, \text{ while } \eta \to \infty. \tag{19}$$

As expressed by [48], to investigate the steady flow consistency $f(\eta) = f_0(\eta)$, $h(\eta) = h_0(\eta)$ and $\theta(\eta) = \theta_0(\eta)$, we write:

$$
\begin{aligned}
f(\eta, \tau) &= f_0(\eta) + e^{-\omega\tau}F(\eta), \\
h(\eta, \tau) &= h_0(\eta) + e^{-\omega\tau}H(\eta), \\
\theta(\eta, \tau) &= \theta_0(\eta) + e^{-\omega\tau}I(\eta),
\end{aligned}
\tag{20}
$$

where ω is the undetermined parameter of eigenvalue, as $F(\eta)$, $H(\eta)$ and $I(\eta)$ are comparatively small to $f_0(\eta)$, $h_0(\eta)$ and $\theta_0(\eta)$. The eigenvalue problem in Equations (16)–(18) leads to an infinite set of eigenvalues $\omega_1 < \omega_2 < \omega_3 \ldots$ that trace a steady flow movement and primary deterioration while ω_1 is positive. However, when ω_1 is negative, the initial development of delays is observed, which exposes the erratic flow. Replacing Equation (20) into Equations (16)–(19), we have:

$$
\frac{\mu_{hnf}/\mu_f}{\rho_{hnf}/\rho_f}\frac{\partial^3 F}{\partial \eta^3} + \left(f_0 + ch_0 - \frac{1}{2}\varepsilon\eta\right)\frac{\partial^2 F}{\partial \eta^2} + (F + cH)\frac{\partial^2 f_0}{\partial \eta^2} + \left(\varepsilon + \omega - 2\frac{\partial f_0}{\partial \eta}\right)\frac{\partial F}{\partial \eta}
$$
$$
+ \frac{\beta_{hnf}}{\beta_f}\Omega I - \frac{\sigma_{hnf}/\sigma_f}{\rho_{hnf}/\rho_f}M\frac{\partial F}{\partial \eta} = 0,
\tag{21}
$$

$$
\frac{\mu_{hnf}/\mu_f}{\rho_{hnf}/\rho_f}\frac{\partial^3 H}{\partial \eta^3} + \left(f_0 + ch_0 - \frac{1}{2}\varepsilon\eta\right)\frac{\partial^2 H}{\partial \eta^2} + \left(\omega - \varepsilon - 2c\frac{\partial h_0}{\partial \eta}\right)\frac{\partial H}{\partial \eta} + (F + cH)\frac{\partial^2 h_0}{\partial \eta^2}
$$
$$
+ \frac{\beta_{hnf}}{\beta_f}\Omega I - \frac{\sigma_{hnf}/\sigma_f}{\rho_{hnf}/\rho_f}M\frac{\partial H}{\partial \eta} = 0,
\tag{22}
$$

$$
\frac{1}{\Pr}\frac{k_{hnf}/k_f}{(\rho C_p)_{hnf}/(\rho C_p)_f}\frac{\partial^2 I}{\partial \eta^2} + \left(f_0 + ch_0 - \varepsilon\frac{1}{2}\eta\right)\frac{\partial I}{\partial \eta} + (F + cH)\frac{\partial \theta_0}{\partial \eta} - \left(\theta_0\frac{\partial F}{\partial \eta} + I\frac{\partial f_0}{\partial \eta}\right)
$$
$$
- \left(c\theta_0\frac{\partial H}{\partial \eta} + cI\frac{\partial h_0}{\partial \eta}\right) + (\omega - 2\varepsilon)I = 0,
\tag{23}
$$

and the boundary conditions are as follows:

$$
F(0, \tau) = 0, \ \frac{\partial F}{\partial \eta}(0, \tau) = 0, \ H(0, \tau) = 0, \frac{\partial H}{\partial \eta}(0, \tau) = 0, I(0, \tau) = 0
$$
$$
\frac{\partial F}{\partial \eta}(\eta, \tau) \to 0, \ \frac{\partial H}{\partial \eta}(0, \tau) \to 0, \ I(\eta, \tau) \to 0, \ \text{as } \eta \to \infty.
\tag{24}
$$

The steady-state flow solutions $f_0(\eta)$ and $\theta_0(\eta)$ were implemented via $\tau \to 0$. Subsequently, the corresponding linearized eigenvalue problem is defined:

$$
\frac{\mu_{hnf}/\mu_f}{\rho_{hnf}/\rho_f}F''' + \left(f_0 + ch_0 - \frac{1}{2}\varepsilon\eta\right)F'' + (F + cH)f_0'' + (\omega - \varepsilon - 2f_0')F'
$$
$$
+ \frac{\beta_{hnf}}{\beta_f}\Omega I - \frac{\sigma_{hnf}/\sigma_f}{\rho_{hnf}/\rho_f}MF' = 0,
\tag{25}
$$

$$
\frac{\mu_{hnf}/\mu_f}{\rho_{hnf}/\rho_f}H''' + \left(f_0 + ch_0 - \frac{1}{2}\varepsilon\eta\right)H'' + (F + cH)h_0'' + (\omega - \varepsilon - 2ch_0')H'
$$
$$
+ \frac{\beta_{hnf}}{\beta_f}\Omega I - \frac{\sigma_{hnf}/\sigma_f}{\rho_{hnf}/\rho_f}MH' = 0,
\tag{26}
$$

$$
\frac{1}{\Pr}\frac{k_{hnf}/k_f}{(\rho C_p)_{hnf}/(\rho C_p)_f}I'' + \left(f_0 + ch_0 - \varepsilon\frac{1}{2}\eta\right)I' + (F + cH)\theta_0' - (F'\theta_0 + f_0'I)
$$
$$
- c(H'\theta_0 + h_0'I) + (\omega - 2\varepsilon)I = 0,
\tag{27}
$$

together with:

$$F(0) = 0, \ F'(0) = 0, \ H(0) = 0, \ H'(0) = 0, \ I'(0) = 0,$$
$$F'(\eta) \to 0, \ H'(\eta) \to 0, \ I(\eta) \to 0, \ \text{as} \ \eta \to \infty. \tag{28}$$

By relaxing a boundary condition, the potential eigenvalues could be estimated [49]. Now, we assume $F'(\eta) \to 0$, consequently, the eigenvalue problems in Equations (25)–(27) are discovered when $F''(0) = 1$, where ω_1 is fixed.

4. Discussion and Results

The nonlinear ordinary differential equations presented in Equations (7)–(10) were solved by using the bvp4c feature in the MATLAB program [50]. The problem of the expressed boundary value is simplified to an ordinary first-order differential equation system, initially. The bvp4c feature is a noteworthy approach commonly exercised by numerous researchers to explain the justification of the reference value. A preliminary forecast of the variations step size and primary mesh point is required beneficial to the necessary response confirmation. In order to find more than one solution, the accurate estimation of boundary layer thickness, together with an early intervention guess is important.

The comparisons of results in Tables 3 and 4 are presented to validate the numerical procedure of the current study with the steady ($\varepsilon = 0$) numerical results from Noor et al. [40] and Eswara and Nath [43] for a different type of fluid. The previous studies by Noor et al. [40] and Eswara and Nath [43] tackled the viscous fluid problem, while the present study implemented the hybrid nanofluid. Further, Eswara and Nath [43] used an implicit finite-difference scheme with a quasilinearization technique while this study applied the bvp4c procedure in the MATLAB programming. It is observed that the present results are in good agreement with the solutions obtained for the steady regular fluid case; thus, this gives us confidence that the computational structure to analyze the hybrid nanofluid flow behaviors and heat transfer in this study can be employed with significant assurance. The key component for determining nanofluid flow behaviors and the efficiency of heat transfer is the organization of compatible single/hybrid nanofluids. Suresh et al. [22] performed the synthesis of Al_2O_3–Cu/H_2O nanocomposite powder and its characteristics for various volume concentrations. In their noteworthy study, nanofluid stability is observed to decrease as volume concentration increases. Since the Al_2O_3–Cu/H_2O hybrid nanofluid is supported in this current work, a different set of ϕ values fraction is limited in between $0.005 \leq \phi \leq 0.02$, corresponds to the work of [51]. The Al_2O_3–Cu/H_2O hybrid nanofluid is selected in this study because of the outstanding work of Suresh et al. [21] in developing an exploration practice to scrutinize the Al_2O_3–Cu/H_2O thermophysical properties. By diffusing the alumina (Al_2O_3) nanoparticle followed by copper (Cu) into H_2O, the Al_2O_3–Cu/H_2O hybrid nanofluid is established with various sums of volume fractions [51,52]. Figures 2–13 unveil the dual solutions existence namely first and second solutions for preferred values of the controlling parameters, that is, the nanoparticles volume fraction (ϕ), the suction parameter (S), the unsteadiness parameter (ε), and the MHD parameter (M) when the mixed convection parameter (Ω) is varied. The non-uniqueness (dual) solutions are perceived to a particular range of Ω_c where Ω_c demonstrates the meeting point of dual solutions or critical point. The separation of flow arises next to the critical point; thus, it is not a laminar flow anymore which automatically failed to fulfil the boundary layer principle. It is noted that the dual solutions are observed in the opposing flow where $\Omega < 0$. An analysis of solution stability is then carried out to assess the efficacy of the solution with the intention of adopting a consistent and practicable solution. Besides, different limiting parameter is used to ensure the accuracy of the solutions and are set to the following extend; $-0.2 \leq \varepsilon \leq -0.6$, $2.0 \leq S \leq 2.4$, and $0.0 \leq M \leq 0.2$. Meanwhile, the value of c is fixed at 0.5 (nodal point).

Table 3. Approximation values of $f''(0)$ and $h''(0)$ by certain values of c when $\phi_1 = \phi_2 = \varepsilon = \Omega = M = S = 0$, and Pr = 0.7.

c	Present Result		Noor et al. [40]		Eswara and Nath [43]	
	$f''(0)$	$h''(0)$	$f''(0)$	$h''(0)$	$f''(0)$	$h''(0)$
1.00	1.311938	1.311938	1.31194	1.31194	1.3128	1.3128
0.75	1.288629	1.164316	1.28863	1.16432	1.2885	1.1642
0.50	1.266866	0.998111	1.26687	0.99811	1.2677	0.9980
0.25	1.247612	0.805137	1.24761	0.80514	1.2475	0.8050
0.00	1.232588	0.570465	1.23259	0.57047	1.2324	0.5706
−0.25	1.225129	0.267950	1.22513	0.26795	1.2249	0.2671
−0.50	1.230195	−0.111500	1.23020	−0.11150	1.2302	−0.1110
−0.75	1.247319	−0.482131	1.24732	−0.48219	1.2489	−0.4975
−1.00	1.271539	−0.794493	1.27277	−0.80950	1.2762	−0.8226

Table 4. Approximation values of $-\theta'(0)$ by certain values of c when $\phi_1 = \phi_2 = \varepsilon = \Omega = M = S = 0$, and Pr = 0.7.

c	$-\theta'(0)$	
	Present Result	Noor et al. [40]
1.00	0.665378	0.66538
0.75	0.623085	0.62308
0.50	0.579670	0.57967
0.25	0.536212	0.53621
0.00	0.495866	0.49587
−0.25	0.467776	0.46778
−0.50	0.470589	0.47059
−0.75	0.507541	0.50755
−1.00	0.562037	0.56595
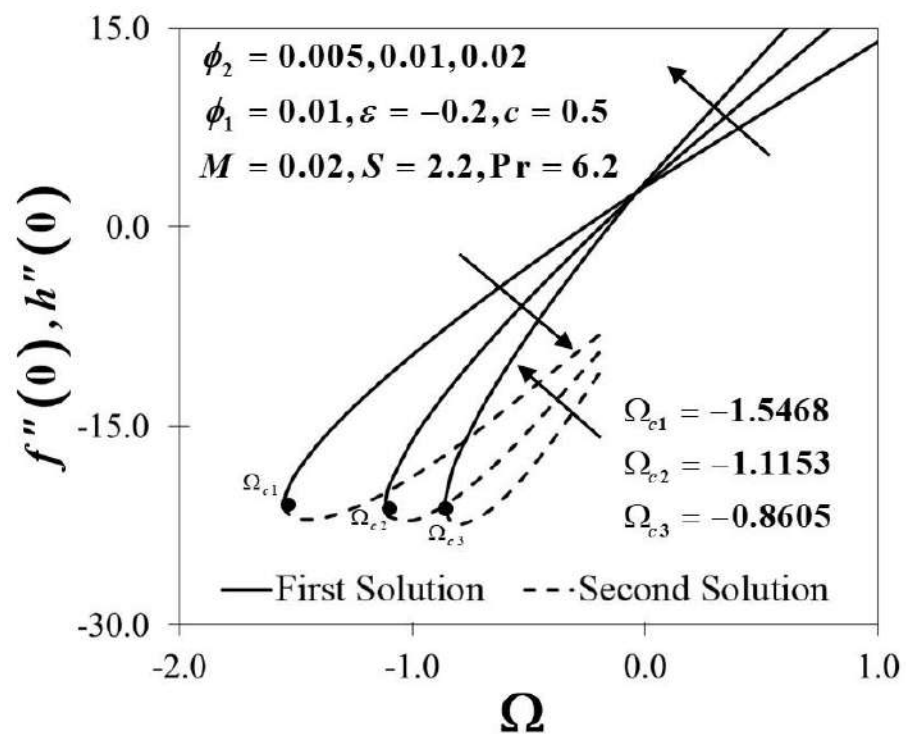
Figure 2. Results of $f''(0), h''(0)$ with $\phi_2 = 0.005, 0.01, 0.02$.
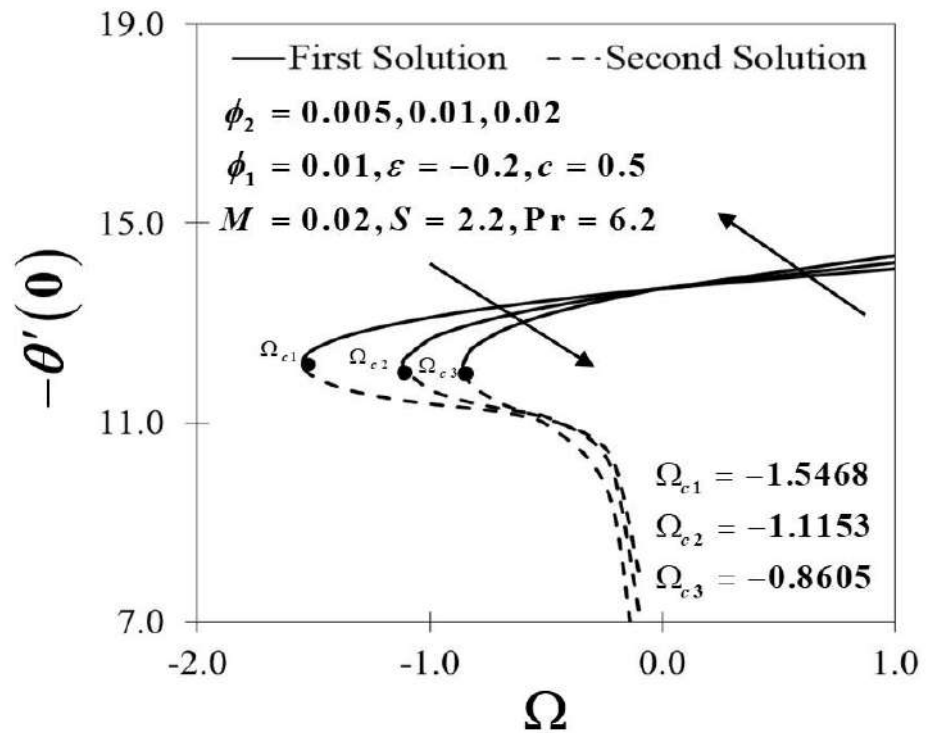
Figure 3. Results of $-\theta'(0)$ with $\phi_2 = 0.005, 0.01, 0.02$.
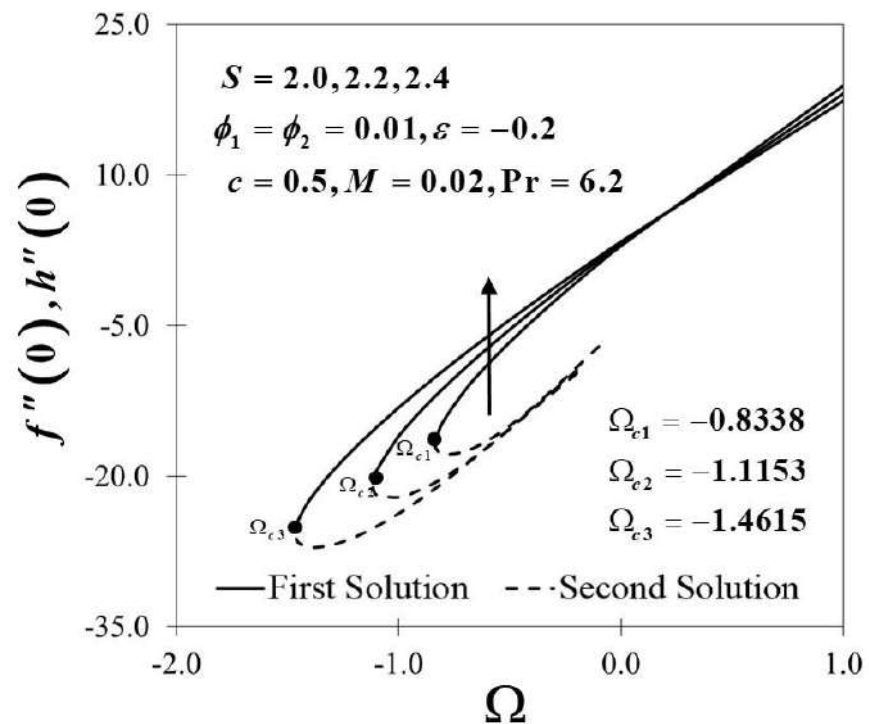
Figure 4. Results of $f''(0), h''(0)$ with $S = 2.0, 2.2, 2.4$.
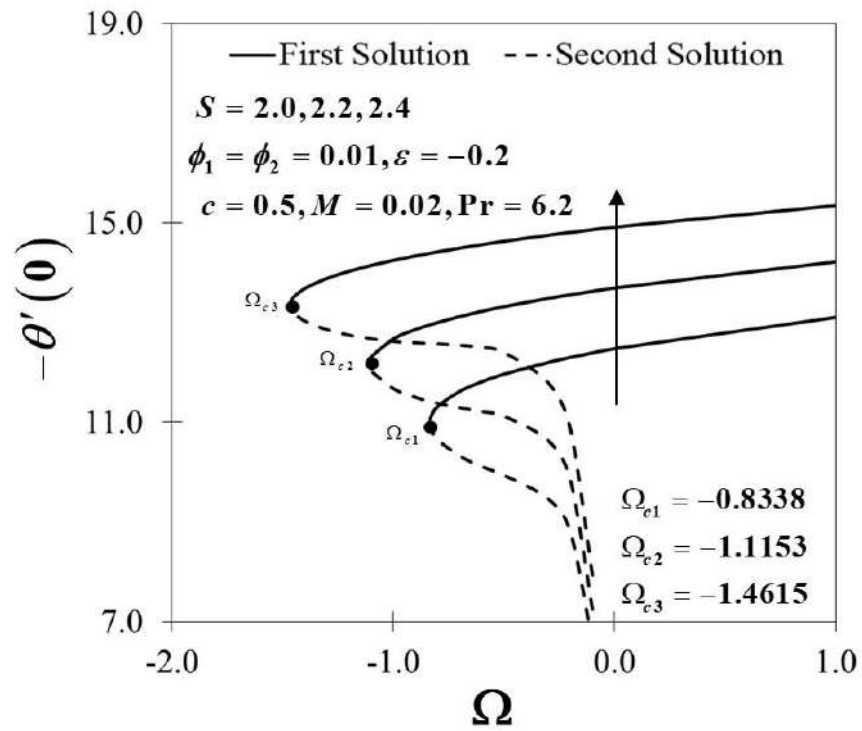
Figure 5. Results of $-\theta'(0)$ with $S = 2.0, 2.2, 2.4$.
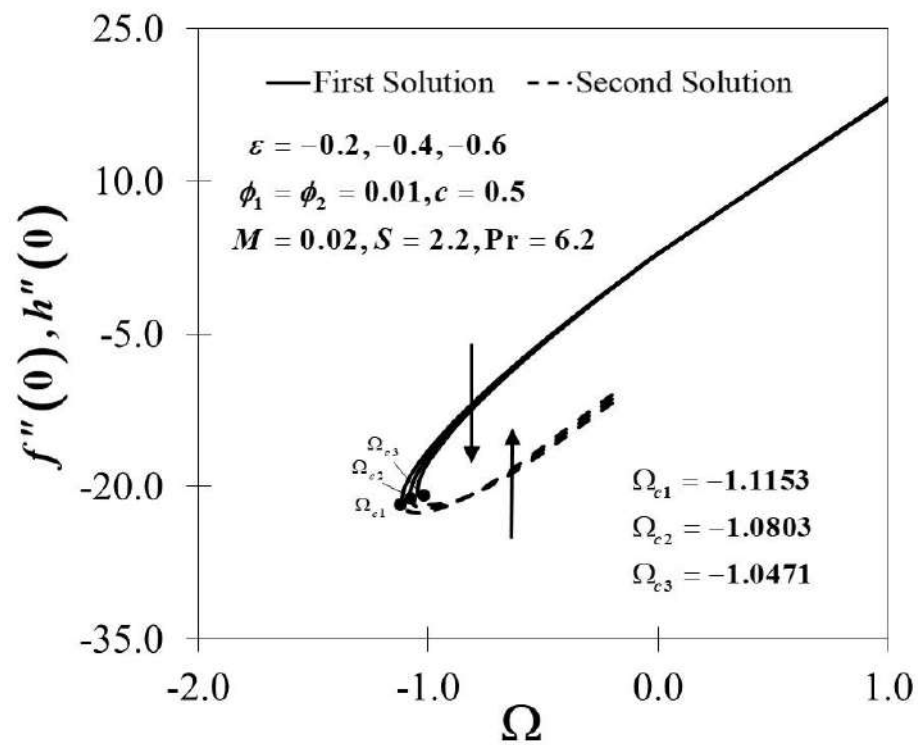
Figure 6. Results of $f''(0), h''(0)$ with $\varepsilon = -0.2, -0.4, -0.6$.
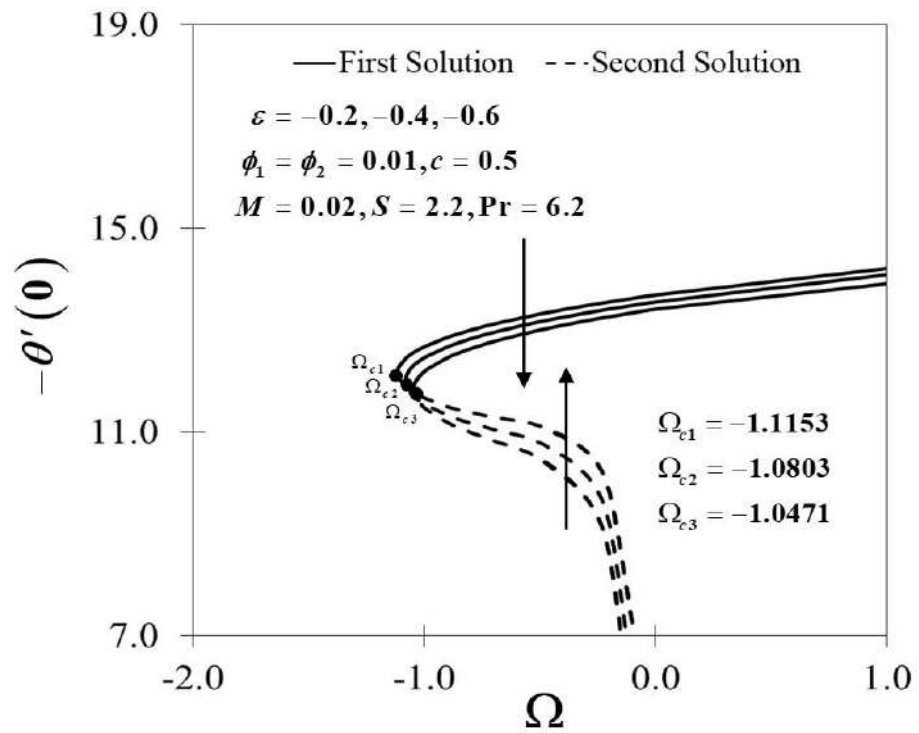
Figure 7. Results of $-\theta'(0)$ with $\varepsilon = -0.2, -0.4, -0.6$.
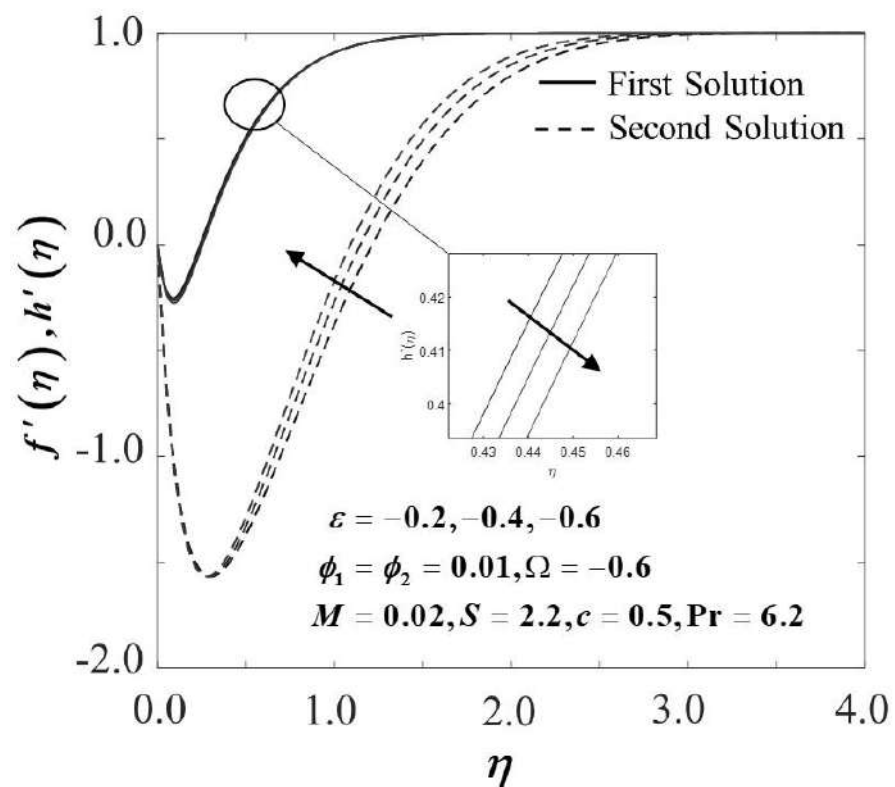
Figure 8. Results of $f'(\eta), h'(\eta)$ with $\varepsilon = -0.2, -0.4, -0.6$.
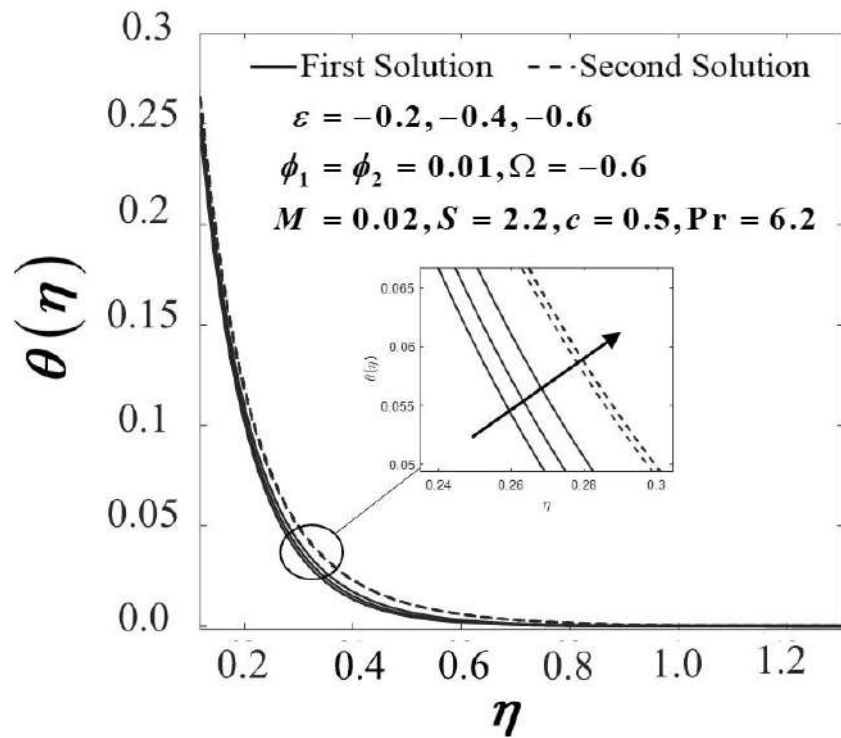
Figure 9. Results of $\theta(\eta)$ with $\varepsilon = -0.2, -0.4, -0.6$.
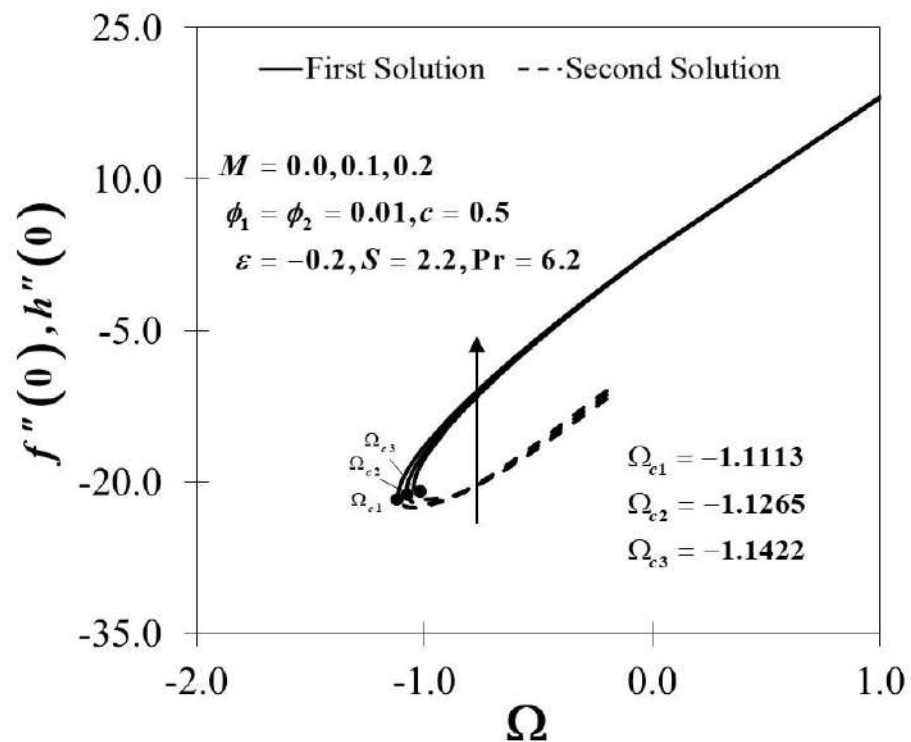
Figure 10. Results of $f''(0), h''(0)$ with $M = 0.0, 0.1, 0.2$.
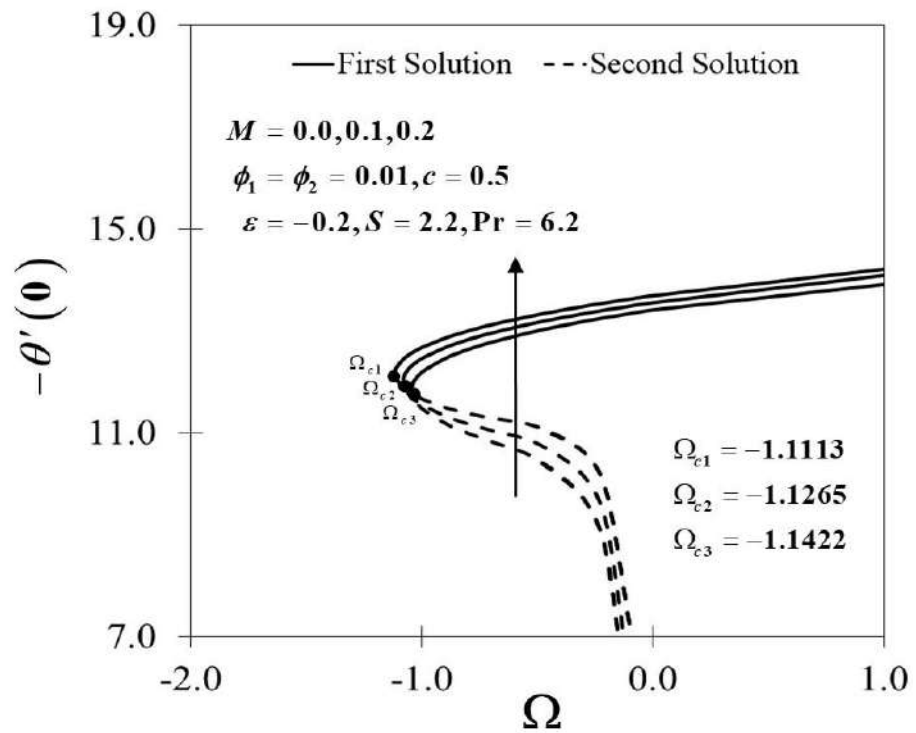
Figure 11. Results of $-\theta'(0)$ with $M = 0.0, 0.1, 0.2$.
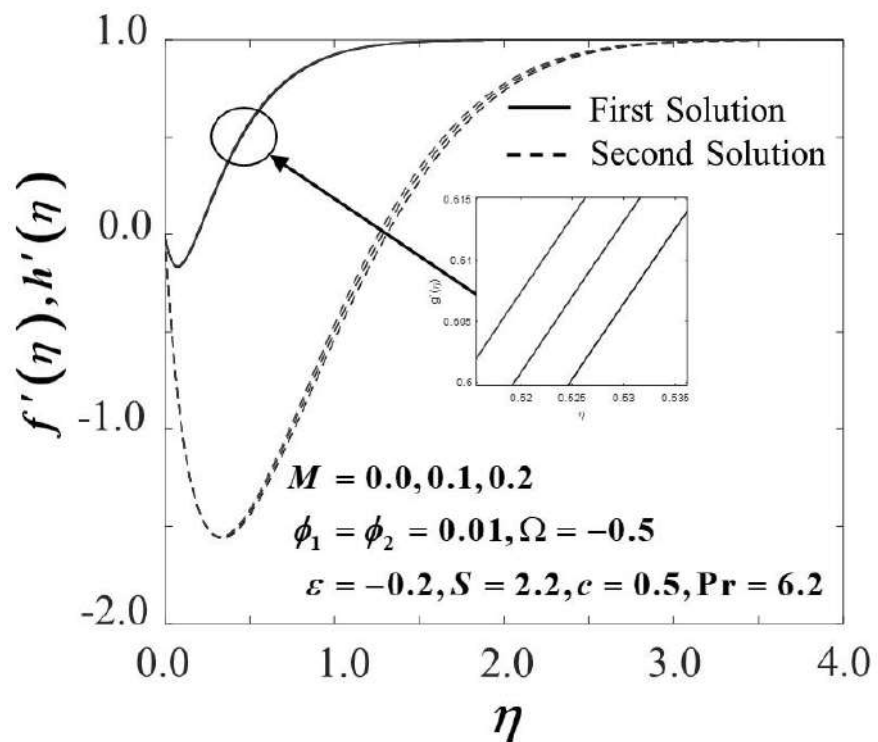
Figure 12. Results of $f'(\eta), h'(\eta)$ with $M = 0.0, 0.1, 0.2$.
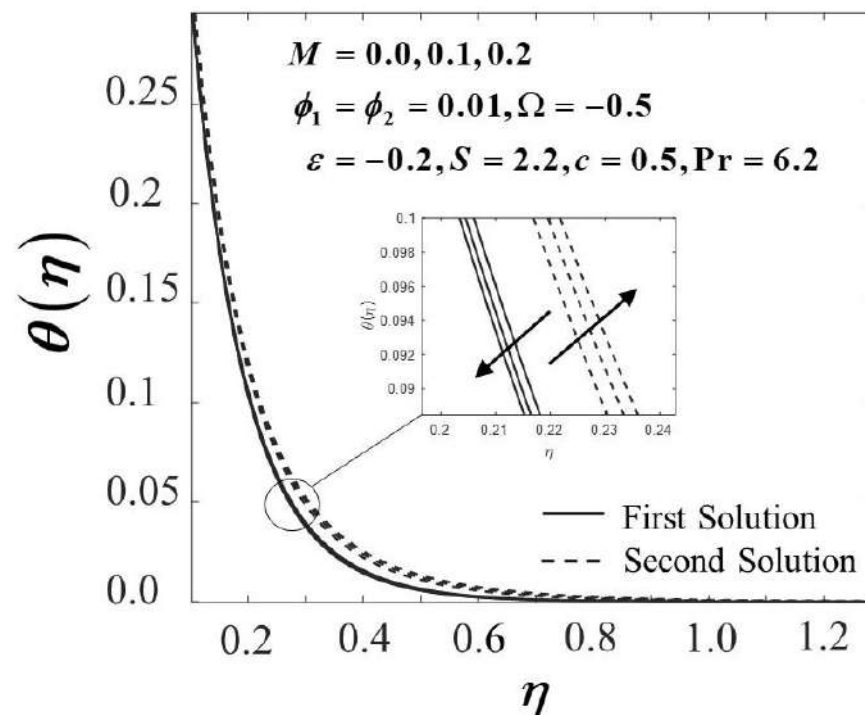
Figure 13. Results of $\theta(\eta)$ with $M = 0.0, 0.1, 0.2$.

The coefficient of skin friction variations $(f''(0), h''(0))$ of Al_2O_3–Cu/H_2O hybrid nanofluid $(\phi_1 = 0.01, \phi_2 = 0.005, 0.01, 0.02)$ and the heat transfer rate $(-\theta'(0))$ towards the mixed convection parameter (Ω) are presented in Figures 2 and 3. Figure 2 expresses the trend of $f''(0)$ and $h''(0)$ toward Ω when ϕ_2 varied. The findings obtained indicate that the scope of mixed convection parameters for which the solution occurs decreases with the inclusion of nanoparticle volume fraction in the first solution while the sheet is shrinking. The same findings have been found in the preceding literature, as stated by Waini et al. [24]. The buoyant force behaves in the same direction as the fluid movement in the assisting flow. This suggests the velocity of fluid flow to enhance thus capable of supporting the buoyant force, thereby, improves shear stress of the permeable surface. In contrast, the consequence of the buoyant force's opposing flow may affect the fluid velocity to become weak, hence affecting the fluid flow to slow down and minimizing the surface shear stress. Further, Figure 2 stresses that when $\Omega = 0$ (static surface), $f''(0), h''(0) = 1$ which explains the lack of frictional drag on the sheet. A diminishing behavior over the first solution of the heat transfer performance or $-\theta'(0)$ when ϕ_2 varied is denoted in Figure 3 and this phenomenon is in contrast with the second solutions. Concisely, the rate of heat transfer decreases as the nanoparticles volume fraction improves in a hybrid nanofluid. This observation suggests that the addition of nanoparticles volume fractions in the boundary layer may minimize the thickness of the thermal boundary layer thus improving the heat flux. Hence, prior to this subsequent case, we may infer that the incorporation of the nanoparticle volume fraction leads to the acceleration of the boundary layer separation.

Figures 4 and 5 expose the effects of various value in S toward Ω past a permeable sheet. The characteristics of $f''(0)$ and $h''(0)$ in Al_2O_3–Cu/H_2O is described in Figure 4. Figure 4 proves an improvement in S will decisively upsurge $f''(0)$ and $h''(0)$ in the first solution. In reality, the suction event may facilitate the boundary layer steadiness. In addition, the suction diminishes the friction of the external flow on the bodies, thereby reducing the boundary layer thickness and magnifying the velocity differential of the permeable sheet by removing the fluid across the low momentum surface. Both solutions convey an increase in $-\theta'(0)$ as S escalates across the permeable sheet, as clarified in Figure 5. Realize that the suction impact permits the molecules of Al_2O_3–Cu/H_2O hybrid nanofluid to occupy the surface and then physically improve the heat transfer rate at the permeable sheet.

The influence of the unsteady parameter ε toward Ω when ε shifts from -0.2 to -0.6 are demonstrated in Figures 6–9. The Al_2O_3–Cu/H_2O hybrid nanofluid characteristic is demonstrated in Figure 6 with respect to the skin friction coefficient $f''(0), h''(0)$ when ε varied in the unsteady case. Figure 6 captures that as ε reduced, the first solution has decreased in $f''(0), h''(0)$ and the second solution has demonstrated a reverse effect. The reduction in ε leads to the expansion of the boundary layer thickness and subsequently declines the velocity gradient of the permeable sheet, hence $f''(0), h''(0)$ diminished. The presence of nanoparticle volume fraction could also initiate the reduction of $f''(0), h''(0)$ because of the rise in Al_2O_3–Cu/H_2O hybrid nanofluid viscosity in the permeable surface. Moreover, according to the generated results in Figure 7, $-\theta'(0)$ is decreased in the first solution which is proportional to the rate of heat transfer, when $\Omega < 0$ (opposing flow) in the permeable sheet as ε reduces. In contrast, the second solution demonstrated an upward trend of $-\theta'(0)$ the values of ε declines. From the current and existing evidence, the authors can infer that the unsteadiness parameter promotes significantly to the degradation of heat transfer. Even so, if multiple control parameters are taken into account, the authors would also like to claim that those effects may vary. The dimensionless profiles of velocity $f'(\eta), h'(\eta)$ with various ε are accessible in Figure 8, where dual velocity profiles are noted. As exemplified in Figure 8, the first solution decreases in proportion to the deteriorating of ε, whereas the second approach revealed contradictory outcomes. In the meantime, the diverse progress of the solution in Figure 8 reflected as well the temperature profile $\theta(\eta)$ with the presence of unsteadiness parameter, which can be seen in Figure 9. Overall, both profiles asymptotically fulfilled the far-field boundary conditions (10) when $\eta_\infty = 4$ is implemented.

Figures 10 and 11 illustrate the magnetic properties impact toward $f''(0), h''(0)$ besides $-\theta'(0)$. Apparently, we recognize that the first solution of $f''(0), h''(0)$ has improved when the values of M rises in the Al_2O_3–Cu/H_2O hybrid nanofluid flow toward Ω, as portrayed in Figure 10. The magnetic field emergence across the electrically conducting fluid contributes to the Lorentz force appearance which prompts endurance to the motion of the fluid particle and therefore increases the fluid velocity (see Figure 12). Furthermore, an escalation of M leads to an intensification of the heat transfer rate as promoted in Figure 11. In short, $-\theta'(0)$ improves in conjunction with the heat transfer rate along the permeable surface. More nanoparticles are drawn to the surface by the Lorentz force ensuing in greater temperature near the permeable sheet. In addition, by expanding the magnetic effect of the working fluid system, the thickness of the boundary layer is increased, thereby reducing the convection mechanism dramatically over the permeable wall surface, as shown clearly in the first solution of Figure 13.

A stability analysis was further carried out by employing the bvp4c application in the MATLAB systems software. The smallest eigenvalues, ω_1 for certain values of Ω when $\phi_1 = 0.01, \phi_2 = 0.02, S = 2.2, M = 0.02, c = 0.5, \varepsilon = -0.2$ are listed in Table 5. The flow represents an erratic flow when ω_1 appears negative because an initial extension of interruptions is proposed. The smallest eigenvalue, ω_1 clarifies the solution stability property to fix the authorizing disturbances, the flow is therefore steady (ω_1 remains positive). It also suggests an early deterioration in the appearance of disruptions.

Table 5. The smallest eigenvalues ω_1 for particular values of Ω.

Ω	ω_1 First Solution	ω_1 Second Solution
-0.8	1.6793	-2.9220
-0.83	1.0506	-2.3993
-0.84	0.7756	-2.1585
-0.848	0.5036	-1.9130
-0.855	0.1818	-1.6126
-0.856	0.1217	-1.5557
-0.857	0.0552	-1.4919

5. Conclusions

A numerical assessment of the unsteady MHD mixed convection stagnation point in Al_2O_3–Cu/H_2O hybrid nanofluid at three-dimensional flow was established in the present work. The engagement of the bvp4c features in the MATLAB programming platform is employed to perform the numerical computation. The result of different regulating parameters, for example, the suction/injection parameter, the nanoparticle volume fraction, the unsteadiness and magnetic parameter were examined. Our analyses suggest that the occurrence of dual solutions is demonstrable for a wide variety of operating parameters, besides the stability analysis permits the first solution reliability. The augmentation in nanoparticle volume concentration surprisingly reduced the coefficient of skin friction and local Nusselt number. Thus, this leads to the conclusion that as the concentration of nanoparticles expands, the heat transfer rate decreases in Al_2O_3–Cu/H_2O hybrid nanofluid for this particular problem. Meanwhile, an upsurge in the suction parameter intensity is capable of boosting the skin friction coefficient and the heat transfer rate of the Al_2O_3–Cu/H_2O hybrid nanofluid. Consequently, a decrement in the unsteadiness parameter decreases the coefficient of skin friction with opposing flow over the permeable surface. On the contrary, it is also reported that improved magnetic control in Al_2O_3–Cu/H_2O hybrid nanofluid escalates the rate of heat transfer. The magnetic fields escalation continues to interrupt the fluid development of the current study. Finally, the stability analysis is executed since the dual solutions are perceived to exist. The first solution's consistency and steadiness were verified by stability analysis, while the second solution is unconvincing and unstable.

Author Contributions: Article preparation, N.A.Z.; Formulation and methodology, N.A.Z.; Research design, N.A.Z., R.N., K.N., and I.P. Analysis of the result, N.A.Z.; Validation, R.N., and K.N.; Review and editing, N.A.Z., R.N., K.N., and I.P. All authors have read and agreed to the published version of the manuscript.

Nomenclature

The following symbols and abbreviations are used in this manuscript:

Roman letters

a, b, c	constants $(-)$
B	transverse magnetic field $(-)$
B_0	strength of the magnetic field $(-)$
C_{fx}, C_{fy}	local skin friction coefficients $(-)$
C_p	specific heat at constant pressure $\left(Jkg^{-1}K^{-1}\right)$
$f(\eta), h(\eta)$	dimensionless velocity function $(-)$
$F(\eta), H(\eta), I(\eta)$	functions $(-)$
Gr	local Grashof number $(-)$
k	thermal conductivity of the fluid $\left(Wm^{-1}K^{-1}\right)$
L	characteristic length of the sheet surface $(-)$
M	magnetic coefficient $(-)$
Nu_x	local Nusselt number $(-)$

$\left(pC_p\right)$	heat capacitance of the fluid $\left(JK^{-1}m^{-3}\right)$
Pr	Prandtl number $(-)$
q_w	surface heat flux $(-)$
Re_x, Re_y	local Reynolds number in the $x-$ and $y-$ axes, respectively (ms^{-1})
S	mass flux parameter $(-)$
t	time (s)
T	fluid temperature (K)
T_{wx}, T_{wy}	variable temperature (K)
T_0	reference temperature (K)
T_∞	surrounding temperature (K)
u, v, w	velocity components along the $x-$, $y-$ and $z-$ axes, respectively (ms^{-1})
$u_e(x)$, $v_e(y)$	velocities of the ambient (inviscid) fluid in the $x-$ and $y-$ axes, respectively (ms^{-1})
w_0	constant mass flux velocity $(-)$
x, y, z	Cartesian coordinates (m)
Greek letters	
β	thermal expansion coefficient $(-)$
δ	constant $(-)$
ε	unsteadiness parameter $(-)$
ϕ_1	nanoparticle volume fractions for Al_2O_3 (alumina) $(-)$
ϕ_2	nanoparticle volume fractions for Cu (copper) $(-)$
η	similarity variable $(-)$
μ	dynamic viscosity of the fluid $\left(kgm^{-1}s^{-1}\right)$
ν	kinematic viscosity of the fluid $\left(m^2s^{-1}\right)$
θ	dimensionless temperature $(-)$
ρ	density of the fluid $\left(kgm^{-3}\right)$
τ	dimensionless time variable $(-)$
τ_{wx}, τ_{wy}	shear stresses or skin frictions in $x-$ and $y-$ axes, respectively $\left(kgm^{-1}s^{-2}\right)$
ω	eigenvalue $(-)$
ω_1	smallest eigenvalue $(-)$
Ω	mixed convection parameter $(-)$
Subscripts	
f	base fluid $(-)$
nf	nanofluid $(-)$
hnf	hybrid nanofluid $(-)$
$s1$	solid component for Al_2O_3 (alumina) $(-)$
$s2$	solid component for Cu (copper) $(-)$
Superscript	
$'$	differentiation with respect to η $(-)$

References

1. Marston, P.G.; Dawson, A.M.; Montgomery, D.B.; Williams, J.E.C. Superconducting MHD Magnet Engineering Program. In *Advances in Cryogenic Engineering*; Springer: Boston, MA, USA, 1980.
2. Katagiri, M. Unsteady magnetohydrodynamic flow at the forward stagnation point. *J. Phys. Soc. Jpn.* **1969**, *27*, 1662–1668. [CrossRef]
3. Pavlov, K.B. Magnetohydrodynamic flow of an incompressible viscous fluid caused by deformation of a plane surface. *Magn. Gidrodin.* **1974**, *4*, 146–147.
4. Takhar, H.S.; Ali, M.; Gupta, A.S. Stability of magnetohydrodynamic flow over a stretching sheet. In *Liquid Metal Magnetohydrodynamics*; Springer: Dordrecht, The Netherlands, 1989; pp. 465–471.
5. Deswita, L.; Junoh, M.M.; Ali, F.; Nazar, R.; Pop, I. Magnetohydrodynamic slip flow and heat transfer over a nonlinear shrinking surface in a heat generating fluid. *Int. J. Eng. Technol.* **2020**, *9*, 534–540. [CrossRef]
6. Fayyadh, M.M.; Naganthran, K.; Md Basir, M.F.; Hashim, I.; Roslan, R. Radiative MHD sutterby nanofluid flow past a moving sheet: Scaling group analysis. *Mathematics* **2020**, *8*, 1430. [CrossRef]
7. Zainal, N.A.; Nazar, R.; Naganthran, K.; Pop, I. MHD flow and heat transfer of hybrid nanofluid over a permeable moving surface in the presence of thermal radiation. *Int. J. Numer. Methods Heat Fluid Flow.* **2020**. [CrossRef]
8. Nisar, K.S.; Khan, U.; Zaib, A.; Khan, I.; Baleanu, D. Exploration of aluminium and titanium alloys in the stream-wise and secondary flow directions comprising the significant impacts of magnetohydrodynamic and hybrid nanofluid. *Crystals* **2020**, *10*, 679. [CrossRef]

9. Zainal, N.A.; Nazar, R.; Naganthran, K.; Pop, I. MHD mixed convection stagnation point flow of a hybrid nanofluid past a vertical flat plate with convective boundary condition. *Chin. J. Phys.* **2020**, *66*, 630–644. [CrossRef]

10. Ramachandran, N.; Chen, T.S.; Armaly, B.F. Mixed convection in stagnation flows adjacent to vertical surfaces. *J. Heat Transfer.* **1988**, *110*, 373–377. [CrossRef]

11. Merkin, J.H. Mixed convection boundary layer flow on a vertical surface in a saturated porous medium. *J. Eng. Math.* **1980**, *14*, 301–313. [CrossRef]

12. Merkin, J.H. On dual solutions occurring in mixed convection in a porous medium. *J. Eng. Math.* **1986**, *20*, 171–179. [CrossRef]

13. Oztop, H.F.; Al-Salem, K.; Pop, I. MHD mixed convection in a lid-driven cavity with corner heater. *Int. J. Heat Mass Transf.* **2011**, *54*, 3494–3504. [CrossRef]

14. Daniel, Y.S.; Daniel, S.K. Effects of buoyancy and thermal radiation on MHD flow over a stretching porous sheet using homotopy analysis method. *Alex. Eng. J.* **2015**, *54*, 705–712. [CrossRef]

15. Jamaludin, A.; Naganthran, K.; Nazar, R.; Pop, I. MHD mixed convection stagnation-point flow of Cu-Al_2O_3/water hybrid nanofluid over a permeable stretching/shrinking surface with heat source/sink. *Eur. J. Mech. B/Fluids* **2020**, *84*, 71–80. [CrossRef]

16. Asadi, A.; Asadi, M.; Rezaniakolaei, A.; Rosendahl, L.A.; Afrand, M.; Wongwises, S. Heat transfer efficiency of Al_2O_3-MWCNT/thermal oil hybrid nanofluid as a cooling fluid in thermal and energy management applications: An experimental and theoretical investigation. *Int. J. Heat Mass Transf.* **2018**, *117*, 474–486. [CrossRef]

17. Esfe, M.H.; Esfandeh, S.; Saedodin, S.; Rostamian, H. Experimental evaluation, sensitivity analyzation and ANN modeling of thermal conductivity of ZnO-MWCNT/EG-water hybrid nanofluid for engineering applications. *Appl. Therm. Eng.* **2017**, *125*, 673–685. [CrossRef]

18. Bahiraei, M.; Mazaheri, N.; Rizehvandi, A. Application of a hybrid nanofluid containing graphene nanoplatelet–platinum composite powder in a triple-tube heat exchanger equipped with inserted ribs. *Appl. Therm. Eng.* **2019**, *149*, 588–601. [CrossRef]

19. Xian, H.W.; Azwadi, N.; Sidik, C.; Aid, S.R.; Ken, T.L.; Asako, Y. Review on Preparation Techniques, Properties and Performance of Hybrid Nanofluid in Recent Engineering Applications. *J. Adv. Res. Fluid Mech. Therm. Sci.* **2018**, *45*, 1–13.

20. Gupta, M.; Singh, V.; Kumar, S.; Kumar, S.; Dilbaghi, N. Up to date review on the synthesis and thermophysical properties of hybrid nanofluids. *J. Clean. Prod.* **2018**, *190*, 169–192. [CrossRef]

21. Suresh, S.; Venkitaraj, K.P.; Selvakumar, P.; Chandrasekar, M. Synthesis of Al_2O_3-Cu/water hybrid nanofluids using two-step method and its thermophysical properties. *Colloids Surf. A Physicochem. Eng. Asp.* **2011**, *388*, 41–48. [CrossRef]

22. Suresh, S.; Venkitaraj, K.P.; Selvakumar, P. Synthesis, characterisation of Al_2O_3-Cu nanocomposite powder and water-based nanofluids. *Adv. Mater. Res.* **2011**, *328–330*, 1560–1567. [CrossRef]

23. Khashi'ie, N.S.; Arifin, N.M.; Pop, I. Non-Darcy mixed convection of hybrid nanofluid with thermal dispersion along a vertical plate embedded in a porous medium. *Int. Commun. Heat Mass Transf.* **2020**, *118*, 104866. [CrossRef]

24. Waini, I.; Ishak, A.; Groşan, T.; Pop, I. Mixed convection of a hybrid nanofluid flow along a vertical surface embedded in a porous medium. *Int. Commun. Heat Mass Transf.* **2020**, *114*, 104565. [CrossRef]

25. Mehryan, S.A.M.; Izadpanahi, E.; Ghalambaz, M.; Chamkha, A.J. Mixed convection flow caused by an oscillating cylinder in a square cavity filled with Cu–Al2O3/water hybrid nanofluid. *J. Therm. Anal. Calorim.* **2019**, *137*, 965–982. [CrossRef]

26. Zainal, N.A.; Nazar, R.; Naganthran, K.; Pop, I. Impact of anisotropic slip on the stagnation-point flow past a stretching/shrinking surface of the Al_2O_3-Cu /H_2O hybrid nanofluid. *Appl. Math. Mech.* **2020**, *41*, 1401–1416. [CrossRef]

27. Waini, I.; Ishak, A.; Pop, I. Hybrid nanofluid flow and heat transfer over a permeable biaxial stretching/shrinking sheet. *Int. J. Numer. Methods Heat Fluid Flow.* **2019**, *30*, 3497–3513. [CrossRef]

28. Hiemenz, K. Die Grenzschicht an einem in den gleichförmigen Flüssigkeitsstrom eingetauchten geraden Kreiszylinder. *Dinglers Polytech. J.* **1911**, *326*, 321–324.

29. Libby, P.A. Heat and mass transfer at a general three-dimensional stagnation point. *AIAA J.* **1967**, *5*, 507–517. [CrossRef]

30. Chiam, T.C. Stagnation-point flow towards a stretching plate. *J. Phys. Soc. Jpn.* **1994**, *63*, 2443–2444. [CrossRef]

31. Takhar, H.S.; Soundalgekar, V.M.; Gupta, A.S. Mixed convection of an incompressible viscous fluid in a porous medium past a hot vertical plate. *Int. J. Nonlinear Mech.* **1990**, *25*, 723–728. [CrossRef]

32. Chamkha, A.J. Hydromagnetic mixed convection stagnation flow with suction and blowing. *Int. Commun. Heat Mass Transf.* **1998**, *25*, 417–426. [CrossRef]

33. Abdelkhalek, M.M. The skin friction in the MHD mixed convection stagnation point with mass transfer. *Int. Commun. Heat Mass Transf.* **2006**, *33*, 249–258. [CrossRef]

34. Jamaludin, A.; Nazar, R.; Pop, I. Three-dimensional mixed convection stagnation-point flow over a permeable vertical stretching/shrinking surface with a velocity slip. *Chin. J. Phys.* **2017**, *55*, 1865–1882. [CrossRef]

35. Naganthran, K.; Basir, M.F.M.; Alharbi, S.O.; Nazar, R.; Alwatban, A.M.; Tlili, I. Stagnation point flow with time-dependent bionanofluid past a sheet: Richardson extrapolation technique. *Processes* **2019**, *7*, 722. [CrossRef]

36. Zainal, N.A.; Nazar, R.; Naganthran, K.; Pop, I. Unsteady stagnation point flow of hybrid nanofluid past a convectively heated stretching/shrinking sheet with velocity slip. *Mathematics* **2020**, *8*, 1649. [CrossRef]

37. Khashi'ie, N.S.; Arifin, N.; Pop, I. Mixed convective stagnation point flow towards a vertical Riga plate in hybrid Cu-Al_2O_3/water nanofluid. *Mathematics* **2020**, *8*, 912. [CrossRef]

38. Khashi'ie, N.S.; Arifin, N.; Hafidzuddin, E.H.; Wahi, N.; Pop, I. Mixed convective stagnation point flow of a thermally stratified hybrid Cu-Al_2O_3/water nanofluid over a permeable stretching/shrinking sheet. *ASM Sci. J.* **2019**, *12*, 17–25.

39. Zainal, N.A.; Nazar, R.; Naganthran, K.; Pop, I. Unsteady three-dimensional MHD non-axisymmetric Homann stagnation point flow of a hybrid nanofluid with stability analysis. *Mathematics* **2020**, *8*, 784. [CrossRef]

40. Noor, A.; Nazar, R.; Naganthran, K. Unsteady mixed convection flow at a three-dimensional stagnation point. *Int. J. Numer. Methods Heat Fluid Flow* **2021**, *31*, 236–250. [CrossRef]

41. Takabi, B.; Salehi, S. Augmentation of the heat transfer performance of a sinusoidal corrugated enclosure by employing hybrid nanofluid. *Adv. Mech. Eng.* **2014**, *6*, 147059. [CrossRef]

42. Ghalambaz, M.; Rosca, N.C.; Rosca, A.V.; Pop, I. Mixed convection and stability analysis of stagnation-point boundary layer flow and heat transfer of hybrid nanofluids over a vertical plate. *Int. J. Numer. Methods Heat Fluid Flow* **2020**, *30*, 3737–3754. [CrossRef]

43. Eswara, A.T.; Nath, G. Effect of large injection rates on unsteady mixed convection flow at a three-dimensional stagnation point. *Int. J. Nonlinear Mech.* **1999**, *34*, 85–103. [CrossRef]

44. Krishnaswamy, R.; Nath, G. Compressible boundary-layer flow at a three-dimensional stagnation point with massive blowing. *Int. J. Heat Mass Transf.* **1982**, *25*, 1639–1649. [CrossRef]

45. Oztop, H.F.; Abu-Nada, E. Numerical study of natural convection in partially heated rectangular enclosures filled with nanofluids. *Int. J. Heat Fluid Flow* **2008**, *29*, 1326–1336. [CrossRef]

46. Cheng, E.H.W.; Özişik, M.N.; Williams, J.C., III. Nonsteady three-dimensional stagnation-point flow. *J. Appl. Mech.* **1971**, *38*, 282–287. [CrossRef]

47. Merrill, K.; Beauchesne, M.; Previte, J.; Paullet, J.; Weidman, P. Final steady flow near a stagnation point on a vertical surface in a porous medium. *Int. J. Heat Mass Transf.* **2006**, *49*, 4681–4686. [CrossRef]

48. Weidman, P.D.; Kubitschek, D.G.; Davis, A.M.J. The effect of transpiration on self-similar boundary layer flow over moving surfaces. *Int. J. Eng. Sci.* **2006**, *44*, 730–737. [CrossRef]

49. Harris, S.D.; Ingham, D.B.; Pop, I. Mixed convection boundary-layer flow near the stagnation point on a vertical surface in a porous medium: Brinkman model with slip. *Transp. Porous Media* **2009**, *77*, 267–285. [CrossRef]

50. Shampine, L.F.; Gladwell, I.; Thompson, S. *Solving ODEs with Matlab*; Cambridge University Press: Cambridge, UK, 2003.

51. Devi, S.P.A.; Devi, S.S.U. Numerical investigation of hydromagnetic hybrid Cu-Al$_2$O$_3$/water nanofluid flow over a permeable stretching sheet with suction. *Int. J. Nonlinear Sci. Numer. Simul.* **2016**, *17*, 249–257. [CrossRef]

52. Devi, S.S.U.; Devi, S.P.A. Numerical investigation of three-dimensional hybrid Cu–Al$_2$O$_3$/water nanofluid flow over a stretching sheet with effecting Lorentz force subject to Newtonian heating. *Can. J. Phys.* **2016**, *94*, 490–496. [CrossRef]